Available online at www.sciencedirect.com
SCIENCE DIRECT®
Journal of Power Sources 123 (2003) 182–189
JOURNAL OF POWER SOURCES
www.elsevier.com/locate/jpowsour

Homogeneous kinetics and equilibrium predictions of coking propensity in the anode channels of direct oxidation solid-oxide fuel cells using dry natural gas

Kevin M. Walters [a], Anthony M. Dean [b,*], Huayang Zhu [a], Robert J. Kee [a]

[a] *Engineering Division, Colorado School of Mines, Golden, CO 80401, USA*
[b] *Department of Chemical Engineering, Colorado School of Mines, Golden, CO 80401, USA*

Received 14 March 2003; accepted 31 March 2003

Abstract

Direct electrochemical oxidation (DECO) solid-oxide fuel cells (SOFCs) offer the potential to generate electrical power from hydrocarbon fuels without the need for upstream fuel processing, such as reforming. However, with pure hydrocarbon fuel entering the flow channels at temperatures typically above 700 °C, fuel pyrolysis can cause molecular-weight growth and the formation of deleterious carbonaceous deposits. This paper, which develops a plug-flow model for fuel (natural gas surrogate) within the anode channels, considers the elementary gas-phase chemical kinetics of fuel pyrolysis and oxidation. It also considers the limiting case of local chemical equilibrium. Formation of cyclic hydrocarbon species is used to indicate deposit propensity. Results show that the likelihood of deposit formation depends strongly on cell temperature, current density, and residence time. Generally speaking, equilibrium favors deposit formation early in the channel whereas, owing to limited residence time, the homogeneous finite-rate kinetics predicts relatively low levels of deposit precursors. In the downstream portions, because of electrochemical oxygen flux though the electrode–electrolyte membrane, chemical equilibrium shifts strongly away from deposit formation to volatile carbon-oxygen species. However, the homogeneous finite-rate kinetics predictions show a continuing increase in coking propensity.

Keywords: Homogenous kinetics; Soild-oxide fuel cells; Direct electrochemical oxidation

1. Introduction

Depending on the particulars of electrode and electrolyte materials, direct electrochemical oxidation (DECO) solid-oxide fuel cell (SOFC) systems typically operate at temperatures between 700 and 900 °C [1]. With a pure hydrocarbon gas entering the anode flow channels at these temperatures, it is well known that the fuel can pyrolyze. These conditions can lead to molecular-weight growth and ultimately to the formation of cyclic and polycyclic aromatic hydrocarbons, which are indicators of a propensity to form carbonaceous deposits. These deposits can damage porous electrode structures, thereby diminishing cell life and performance. Deposit formation depends on temperature and residence time as well as the local chemical composition of the stream. Pure fuel enters the anode channels and is electrochemically oxidized, producing H_2O and CO_2. Increasing product concentrations toward the downstream end of the anode channel possibly inhibit fuel pyrolysis by altering residence time and reaction rates.

The principal objective of this work is to characterize the gas-phase chemistry along the anode channel of a DECO-SOFC as a function of cell design and operating conditions. The cell current density determines the rate at which hydrocarbon fuel is electrochemically converted to H_2O and CO_2. Along with current density, the fuel flow rate and channel dimensions affect the residence time and chemical composition, thus altering the likelihood of molecular-weight-growth chemistry.

The homogeneous kinetic model considers a large, elementary reaction mechanism that is well suited to understanding fuel stability and molecular-weight growth for gas-phase hydrocarbon systems. In particular, we look for the production of cyclic hydrocarbon molecules as indicators of deposit formation, much as these species are used as indicators of soot production in combustion processes [2]. Equilibrium calculations are performed along the channel, providing a basis for comparison between the kinetic prediction and local thermodynamic equilibrium.

* Corresponding author. Tel.: +1-303-273-3643; fax: +1-303-273-3730.
E-mail address: amdean@mines.edu (A.M. Dean).

0378-7753/$ – see front matter © 2003 Elsevier Science B.V. All rights reserved.
doi:10.1016/S0378-7753(03)00536-6

In addition to gas-phase reactions, heterogeneous kinetics play a significant role in electrochemical, oxidation and pyrolysis reaction pathways. However, due to the complexity of DECO-SOFC systems, we have focused on the homogenous kinetics in this work. This is done in part to identify the relative magnitude of homogeneous fuel chemistry and the effects of electrochemical oxidation. Local equilibrium predictions provide some indication of what might happen to the fuel stream in the presence of catalytically accelerated reactions.

1.1. Kinetic and equilibrium models

Koh et al. [3] presented an equilibrium model for solid carbon deposition in SOFC systems using dry hydrocarbon fuels. The relationship between current density and the flux of oxygen atoms into the system, along with the design and operating conditions of the cell, formed the basis for a map of equilibrium solid carbon as a function of system parameters. However, this work did not account for finite-rate kinetics in the fuel stream. Consideration of both kinetics and chemical equilibrium is essential to gain an improved understanding of the fuel chemistry in DECO-SOFC systems. The kinetic model, when combined with a fluid-flow model, predicts spatial variation in gas-phase species composition along the channel. A free-energy minimization, given the temperature, pressure and local atomic species distribution from the solution to the kinetic model, gives the chemical equilibrium state of the local mixture at a particular point in the channel.

1.2. DECO-SOFC background

DECO type SOFC systems are a rapidly advancing technology, potentially offering a highly efficient alternative for electrical power generation from hydrocarbon fuels without upstream fuel preparation such as reforming or water addition [4]. Fig. 1 illustrates some of the essential elements typical of a planar SOFC architecture. The heart of the cell is the electrochemically active membrane–electrode assembly (MEA), which consists of a dense ceramic electrolyte sandwiched between porous, ceramic-metal composite electrodes. The electrolyte is impervious to gas flow, but is an oxygen-ion (O^{2-}) conductor. Reactants and products are transported through typically rectangular flow channels, with a cross-sectional area in the order of 0.5–1.0 mm^2. The length and number of channels varies, depending on the active MEA area and hence the power level of the stack [5]. Usually, several tens of cell layers are stacked and electrically connected in series. Because an individual cell layer produces an output voltage approximately 0.5 V at peak power density, the stack configuration increases the operating voltage to more practical levels.

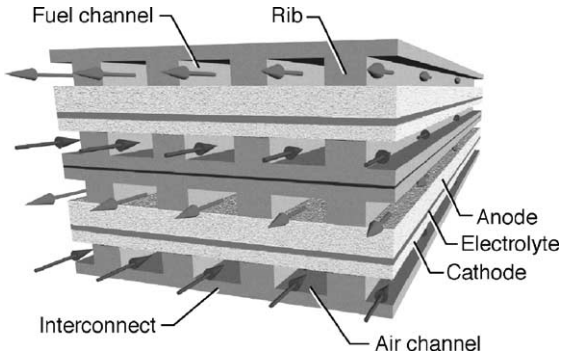

Fig. 1. Illustration of a segment of two fuel-cell layers, including the electrode–electrolyte assembly (MEA), the interconnect, and the flow channels for fuel and air. A counter-flow situation is illustrated here, but co-flow and cross-flow configurations are also common.

In a methane-fed DECO-SOFC, there are two principal electrochemical reactions. On the cathode side of the electrolyte, O_2 is reduced,

$$O_2 + 4e^- \rightleftharpoons 2O^{2-}, \tag{R1}$$

producing negatively charged ions that are transported through the electrolyte to the anode interface. At the electrolyte–anode interface, electrochemical oxidation reactions occur, which can be expressed globally for methane as

$$CH_4 + 4O^{2-} \rightleftharpoons 2H_2O + CO_2 + 8e^-, \tag{R2}$$

depleting fuel and producing CO_2 and H_2O. While homogeneous reactions produce other species that are known to participate in electrochemical oxidation reactions (e.g. H_2 and CO) under these conditions very little CH_4 is converted to such species in the gas phase. Electrochemical oxidation also frees electrons from the charged species, producing an electrical current through an external circuit. While the actual process involves many reaction steps and complex heterogeneous electrochemistry at the three-phase boundaries, the global representation is sufficient to account for the electrochemically produced product species on the gas-phase chemistry in the flow channels.

Based on the global anodic electrochemical reaction (R2), the molar fluxes between the fuel stream and the MEA of the methane–SOFC system at a local current density of i_e can be represented as,

$$J_{CH_4} = -\frac{i_e}{8F}, \qquad J_{CO_2} = \frac{i_e}{8F}, \qquad J_{H_2O} = \frac{i_e}{4F}, \tag{1}$$

where F is the Faraday constant. As the electric cell potential E_{cell} across the MEA structure can be assumed to be constant along the channel due to the excellent electric conductivity of the interconnect, the current density i_e may vary along the channel as a result of fuel and oxidizer consumption. However, the relationship between the current density i_e and the electric cell potential E_{cell} is complex [6]. It depends on all the polarization losses (i.e. concentration, activation, and ohmic polarizations) across the MEA structure, thereby depending on the material properties and micro-structures, and operating conditions, particularly on the fuel and oxidizer compositions. To incorporate the effect of fuel consumption along the channel into the current model, the following simple model for the current density i_e

is used,

$$i_e = i_e^0[CH_4]^\gamma. \quad (2)$$

where i_e^0 is a constant, $[CH_4]$ is the local molar concentration of CH_4 in the fuel stream. The exponent γ is a constant determining the order dependence of i_e on CH_4 concentration.

2. Model structure

The Reynolds number (based on a characteristic channel diameter) for typical anode-channel flow is of order unity. Since the entry length for small Reynolds numbers is short compared to the channel length, we make a plug-flow approximation that considers only the mean axial velocity. Variations in temperature and composition across the channel are assumed to be negligible. This assumption was justified by a boundary–layer model that showed negligibly small radial variation in composition or temperature across the channel width. We chose to neglect diffusive transport in the axial direction, which is consistent with the model developed by Iwata et al. [7]. Furthermore, only isothermal flows are discussed in this analysis, although temperature variation would affect the reaction chemistry and impact cell performance. We assume nominal atmospheric pressure throughout the stream. The plug-flow model, which is based on the PLUG software [8] that is in the Chemkin-III package, has been extended to accommodate the electrochemically driven flux of reactants (CH_4) and products (H_2O and CO_2) that enter or leave the channel. Detailed chemical kinetics are handled through the Chemkin-III [9] and Surface Chemkin-III [10] software interfaces.

2.1. Governing equations

Fig. 2, which depicts a control volume inside an anode channel, serves as the framework within which the needed conservation equations are derived. The control volume has differential length dz along the flow direction, but spans the channel's width and height.

Restricting attention to steady, one-dimensional, plug flow, the mass conservation equation is expressed as,

$$A_c \frac{d(\rho u)}{dz} = a'_e \sum_{k=1}^{K} J_k W_k + a'_s \sum_{k=1}^{K} \dot{s}_k W_k. \quad (3)$$

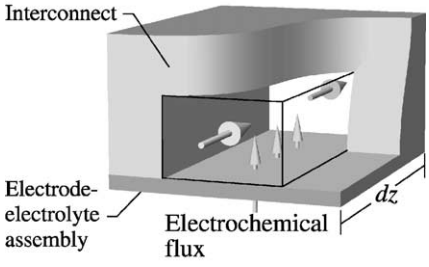

Fig. 2. Illustration of a control volume inside the fuel channel with the H_2O and CO_2 flux coming through the anode into the fuel stream.

The species molecular weights are given as W_k and $\dot{s}_k$ are the molar production rate of gas-phase species by surface reaction. Although the results presented in this paper neglect catalytic chemistry, the terms are retained so that the model can be extended to include surface chemistry.

In Eq. (3), A_c represents the cross-sectional area of the channel. The parameter a'_e is the electrochemically active area per unit length of channel (i.e. the perimeter available for electrochemistry). In Fig. 2, a'_e would be the width of the channel floor plus the width of the active surface under the interconnect ribs. The parameter a'_s is area per unit length (i.e. the perimeter) of the channel wall that is available for heterogeneous surface chemistry.

The surface-chemistry term $\sum \dot{s}_k W_k$ can only provide a net mass loss or gain to the channel flow if there is deposition on the wall. Alone, catalysis can only alter the chemical composition of the flow, but cannot alter the mass flow rate. It should be noted that the surface-chemistry term in the overall continuity equation vanishes for purely catalytic reaction where there is no net mass exchange with the surface. However, the individual contributions to the summation are important in the species continuity equations.

For each species k, the general conservation equation may be stated as

$$A_c \rho u \frac{dY_k}{dz} = a'_e \left(J_k W_k - Y_k \sum_{k=1}^{K} J_k W_k \right) + a'_s \left(\dot{s}_k W_k - Y_k \sum_{k=1}^{K} \dot{s}_k W_k \right) + A_c \dot{\omega}_k W_k. \quad (4)$$

where Y_k represent the mass fractions, $\dot{\omega}_k$ are the molar production rates by homogeneous reactions, and W_k are the molecular weights.

The conservation of momentum is expressed as

$$\rho u \frac{du}{dz} = -\frac{u}{A_c} \left(a'_e \sum_{k=1}^{K} J_k W_k + a'_s \sum_{k=1}^{K} \dot{s}_k W_k \right) - \frac{dp}{dz} - \frac{P}{A_c} \tau_w. \quad (5)$$

The wall shear stress, τ_w, is represented here in terms of the friction factor f as

$$f = \frac{\tau_w}{(1/2)\rho u^2}. \quad (6)$$

For the low-Reynolds number channel flow, the product $Re\, f$ is a constant. For rectangular channels, the value of $Re\, f$ (based on the hydraulic diameter, D_h) depends on the channel aspect ratio $\alpha = H/W$ as

$$Re\, f \approx 13.74 + 10.38 \exp\left(-\frac{3.4}{\alpha}\right), \quad Re = \frac{\rho u D_h}{\mu}. \quad (7)$$

The principal role of the momentum equation in the plug-flow analysis is to determine the pressure profile along the length of the channel. Assuming that the thermodynamic

pressure is nearly uniform for the purposes of evaluating density, chemical and thermodynamic properties, the continuity equations can be decoupled from the momentum equation. In other words, for a given pressure, the velocity and species profiles can be determined from the continuity equations alone.

An ideal-gas equation of state is used to evaluate the mass density, ρ, in terms of pressure and species mass fractions,

$$\rho = \frac{p}{RT}\frac{1}{\sum_{k=1}^{K} Y_k / W_k}. \quad (8)$$

Because the flow is presumed to be isothermal, an energy equation is not required. Nevertheless, it should be noted that it is not uncommon in practice to have temperature variations along the length of a flow channel. The details of such temperature variations depend strongly on system-level considerations like the stack size and insulation strategies. Since the present model is concerned with a single channel, it is not practical to incorporate these system-level influences.

2.2. Elementary gas-phase mechanism

The detailed chemical mechanism used in this analysis is an extension of one published earlier [11] to describe the kinetics of C_4 and smaller fuel species. It has been extended to selected C_6 species (*n*-hexane, 2,3-dimethyl-butane, and cyclohexane) by allowing for both dissociation and hydrogen abstraction from the parent fuel species. The radicals formed from the parent in these processes are then allowed to undergo beta-scission, isomerization, and bimolecular reactions. This sequence is continued until the resulting products are already included in the base C_4 mechanism. The underlying C_4 mechanism has also been modified to reflect improved understanding. One such modification reflects a detailed analysis of propargyl radical recombination. This mechanism is substantially similar to one previously used to model the effect of temperature on soot formation in diesel engines [2].

The mechanism includes many pressure-dependent reaction rate coefficients and the estimates for atmospheric pressure are used for the current calculations. Pressure dependencies arise in those reactions in which a new chemical bond is formed, depositing the bond energy in the newly-formed molecule. The subsequent fate of this species depends upon the relative rates of the various uni-molecular reaction pathways (dependent on temperature) to the collisional stabilization rate (dependent on pressure). The procedure for estimation of these pressure-dependent rate coefficients for the various product and stabilization channels has been previously described [12].

Hydrogen-abstraction reactions included in the mechanism were assigned rate coefficients using a procedure also described previously [13]. These rate coefficients are estimated by relating the parameters for a specific reaction type (e.g. abstractions by OH) to that for a well characterized hydrocarbon analog (e.g. OH + C_2H_6). Consistent use of such reference reactions avoids propagating whatever inconsistencies are present in published compilations. Moreover, this approach accounts for the different temperature dependencies found for various types of hydrogen abstractions. It is now well recognized [14] that many hydrogen-abstraction reactions show upward curvature in their Arrhenius plots, leading to appreciably higher rate coefficients at high temperatures than one would estimate from a linear extrapolation of low-temperature measurements. Such temperature dependencies have to be included in order to predict reliable rate coefficients under high-temperature conditions. A convenient way to include this dependence is to express the rate constant in modified Arrhenius form,

$$k = AT^{\beta}\exp\left(-\frac{E_a}{RT}\right), \quad (9)$$

which is consistent with Transition State Theory.

The reaction mechanism proposed by Frenklach and Warnatz [15] was employed for describing formation of the second aromatic ring and further cyclizations and oxidation. The ring-growth sequence is continued up to cyclopentacoronene in this model. The aromatic rings grow by H-abstraction–C_2H_2-addition reaction sequence. These reactions were included to provide a pathway to large polynuclear aromatics (PAH), which were considered to be the species that could potentially form deposits.

All reactions are considered reversible, with the reverse rate coefficients computed using calculated temperature-dependent equilibrium constants. The thermodynamic data required to determine the equilibrium constants were obtained using group additivity [16,17] for those species where experimental thermodynamic data were not available.

This hydrocarbon pyrolysis and oxidation mechanism is considerably larger than the previous C_4 model. The C_4 mechanism included 447 reactions among 127species, whereas the current mechanism contains 2498 reactions among 291 species.

Fig. 3 illustrates some of the critical steps along the pathway from a parent fuels species (e.g. ethane) to a deposit precursor (e.g. cyclopentene). A series of abstraction, beta-scission and addition/recombination reactions result in a stable five-carbon ring. Under the appropriate conditions, similar reaction steps can continue to produce larger molecules.

2.3. Solution method

The governing equations may be a system of ordinary differential equations (ODE) or differential-algebraic equations (DAE), depending on the details of the surface chemistry. For the results discussed in this paper, the governing equations are a set of ordinary differential equations. In more complex surface-reaction mechanisms, which incorporate surface site fractions as dependent variables, the equations become differential-algebraic equations. In either case, the DASSL [18,19] software is used to solve the

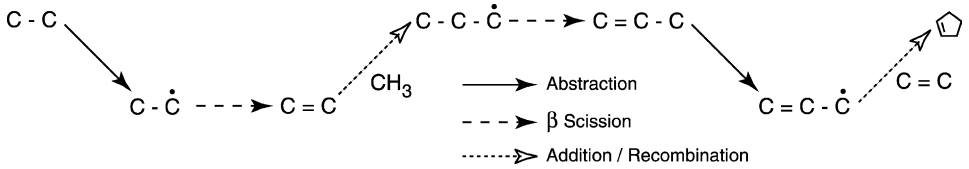

Fig. 3. Primary reaction pathway from ethane to cyclopentene.

system. DASSL implements a variable order, variable step size, implicit method based on the backward differentiation formulas. It automatically adjusts the step size to control local truncation error according to a user-specified tolerance.

In addition to the species distributions predicted by the kinetics simulation, the local equilibrium state is also determined. The equilibrium prediction, which constrains pressure and temperature, begins with the kinetically predicted species distribution at a particular point in the channel. The free-energy minimization procedure is accomplished with the Equil [20] software, which uses a Chemkin-III interface to STANJAN-III [21]. The equilibrium evaluation considers all the species that are included in the kinetics reaction mechanism. Since pure carbon (graphite) is not included in the kinetics it is also not included in the equilibrium prediction.

2.4. Parameters and boundary conditions

The results in this paper are based on a 10 cm long rectangular channel that is 0.5 mm high and 1.0 mm wide. Assuming 1 mm spacing between channels, the electrochemically active area per unit length of channel is $a'_e = 2$ mm. Inlet velocities of 40, 60 and 150 cm/s are used.

The temperature profile along the channel is uniform, with calculations reported at 800 and 900 °C. While the model is capable of various temperature profiles, these effects are not explored in this work. The feed gas is 95% CH_4/5% C_2H_6, although we assume that only methane is electrochemically oxidized. Ethane, commonly found in commercial natural gas, participates in initiation reactions and tends to accelerate molecular-weight-growth chemistry.

The electrochemical performance of a particular system requires knowledge of the system architecture, materials, charge-exchange kinetics, and the associated overpotential losses. Although none of these are specifically considered in this paper, knowledge of the current-density profile is sufficient to determine the product fluxes into the anode channel. We consider two limiting cases: one in which the current density is uniform along the channel and the other in which the current density has first-order dependence on the fuel concentration. The order-dependence parameter γ in Eq. (2) is 0 for a uniform current density and 1 for a current density that is proportional to the local CH_4 concentration. The value of i_e^0 is chosen to provide a uniform current density of 600 mA/cm^2 for $\gamma = 0$ and a current density of 600 mA/cm^2 at the inlet for $\gamma = 1$. These limiting electrochemical assumptions are sufficient to achieve our objective of predicting the role of homogeneous kinetics in coking propensity. The assumptions are clearly not sufficient to predict cell performance generally.

3. Results

By varying the inlet velocity, and hence the fuel flow rate, both residence times and composition profiles are changed significantly. Increasing the flow rate increases the flux of fuel down the channel relative to the flux of electrochemical reactants and products through the MEA active area. As shown in Fig. 4 for $\gamma = 0$, higher fuel flow rates lead to generally higher CH_4 concentrations and lower H_2O and CO_2 concentrations. Residence times for these conditions are 158, 115 and 56 ms for inlet velocities of 40, 60 and 150 cm/s, respectively. Though some CH_4 reacts homogeneously, depletion of CH_4 is dominated by electrochemistry. H_2 and CO mole fractions are less than 0.01 for all sets of parameters and boundary conditions, supporting the assumption that very little CH_4 is converted homogeneously to these electrochemically active species. Rather, gas-phase CH_4 depletion occurs mainly along pyrolysis reaction pathways.

For a cell operating at 900 °C, several cyclic hydrocarbon species are produced in appreciable quantities, with cyclopentene appearing in the highest concentration. Fig. 5 shows the mole fraction of cyclopentene for the various

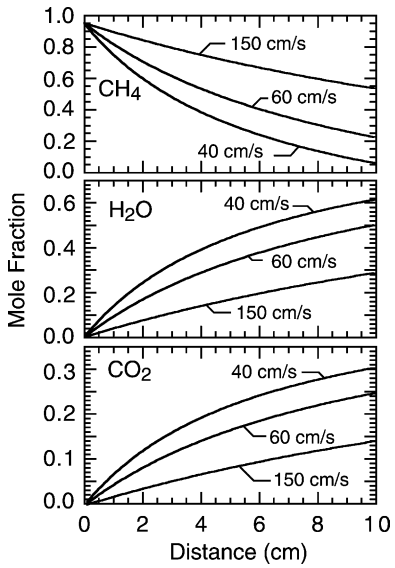

Fig. 4. Profiles of CH_4, H_2O and CO_2 mole fractions with various inlet velocities at 900 °C and $\gamma = 0$.

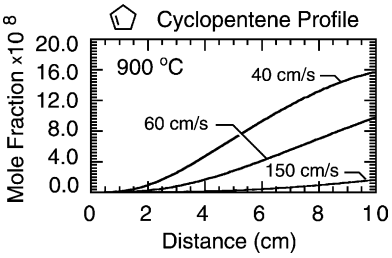

Fig. 5. Profiles of cyclopentene mole fraction with various inlet velocities at 900 °C and $\gamma = 0$.

inlet velocities and $\gamma = 0$. The lower flow rates lead to much higher levels of cyclopentene, despite the elevated concentration of H_2O and CO_2. This is mainly attributed to a significant increase in residence time and correspondingly an increase in the homogeneous pyrolysis. The kinetic predictions for this scenario indicate that deposit precursor formation can be inhibited by reducing the residence time, but this implies a decrease in fuel utilization.

Directly comparing the kinetic prediction to the local equilibrium solution provides better basis for understanding the progression of molecular-weight growth chemistry than kinetics alone. All species with five or more carbon atoms and cyclic or polycyclic structure are considered to be indicators of a propensity to form deposits. While the coking precursors produced in the kinetic model are typically single-ring hydrocarbons, the equilibrium model tends to predict high concentrations of multi-ring aromatics. To compare the results of the two models, the analysis is simplified by looking at specific groups of molecular species. The fractional carbon content F_C is defined as the ratio of the number of carbon atoms in deposit precursor species to the total number of carbon atoms.

As seen in Fig. 6, the kinetic and equilibrium predictions for coking propensity are substantially different. The kinetic model indicates that the greatest likelihood for deposit formation is near the end of the channel, where the fuel stream has experienced the longest residence time. The fraction of carbon in precursors is much higher for cases with longer

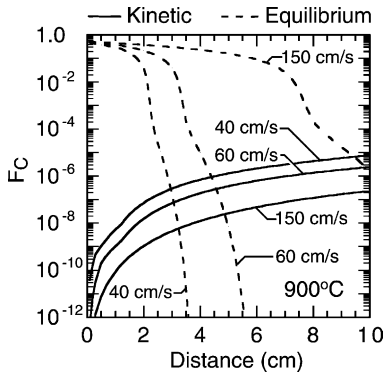

Fig. 6. Profiles of fractional carbon content in deposit precursors for both kinetic and equilibrium models with various inlet velocities at 900 °C and $\gamma = 0$.

residence times. At higher flow rates, the equilibrium predictions indicate a much higher propensity to form deposits than the kinetic model, with the highest fraction of carbon atoms in deposit precursors near the channel inlet where there is very little oxygen in the system. However, note the dramatic drop in equilibrium deposit precursors further downstream. This is due to the increased oxygen atom content in the stream as more H_2O and CO_2 enter the channel. Interestingly, the kinetic model and equilibrium calculations crossover due to slow rates for processes involving molecular-weight growth.

Hydrogen abstraction from water by radical species $\dot{R}$, such as

$$H_2O + \dot{R} \rightleftharpoons RH + OH, \quad \text{(R3)}$$

produce OH radicals which are capable of oxidizing large molecules. However, the rate of (R3) is very low under these conditions, making this pathway for deposit precursor destruction ineffective. Thus, the deposit precursors continue to form, but at a slower rate than near the inlet. As the flow rate increases, the shorter residence time and change in stream composition cause the crossover point to shift downstream. The homogeneous kinetics suggest increases in deposit precursor concentration further down the channel in spite of the increased concentration of H_2O and CO_2. One might be able to take advantage of the increased oxygen content near the outlet by introducing an active catalyst to bring the system to equilibrium more quickly.

As expected, when the assumed value of γ increases from 0 to 1, the rate at which electrochemical reactions convert CH_4 to H_2O and CO_2 decrease in downstream portions of the channel as CH_4 is depleted. The difference in electrochemical oxidation rate manifests itself in the relatively high CH_4 mole fraction and relatively low H_2O and CO_2 mole fractions shown in Fig. 7. For inlet velocities of 40, 60 and

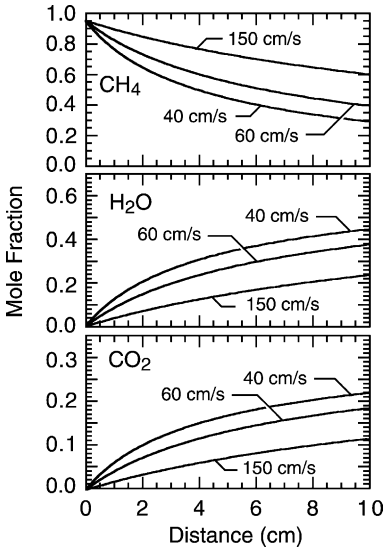

Fig. 7. Profiles of CH_4, H_2O and CO_2 mole fractions with various inlet velocities at 900 °C and $\gamma = 1$.

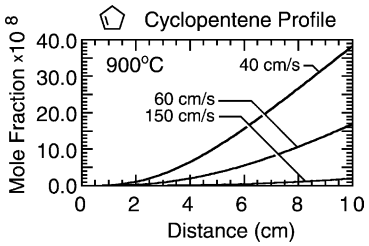

Fig. 8. Profiles of cyclopentene mole fraction with various inlet velocities at 900 °C and $\gamma = 1$.

150 cm/s, the residence times are increased to 182, 124 and 57 ms, respectively. The increased residence time and decrease in dilution by H_2O and CO_2 lead to significantly higher levels of cyclopentene in the fuel stream. Comparing Figs. 5 and 8 shows that the cyclopentene mole fraction more than doubles when the functional dependence of current density changes from zero to first order.

Fig. 9 shows comparisons between kinetic and equilibrium solutions when the electrochemistry is first order in the fuel concentration, $\gamma = 1$. Not only are both the kinetic and equilibrium predictions for coking propensity higher than that for $\gamma = 0$, the higher order dependence leads to a decrease in the current density as CH_4 is depleted. The decreased current density causes a substantially lower average power output.

The kinetic model predicts a very strong temperature dependence, as seen in a comparison between the 900 °C calculation in Fig. 6 and an analogous calculation at 800 °C shown in Fig. 10. The 100 °C temperature reduction decreases the kinetically predicted F_C by several orders of magnitude. The equilibrium calculation changes as well, but with a less dramatic decrease in coking propensity. While decreasing the operating temperature is desirable for minimizing deposits in the anode, this is not necessarily a practical solution because thermally activated electrochemical processes are less effective at lower temperatures. The optimal operating temperature must consider the competition between coking propensity and electrochemical performance.

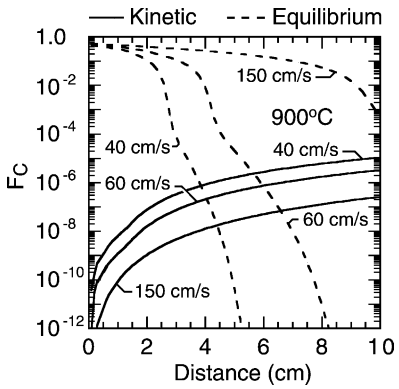

Fig. 9. Profiles of fractional carbon content in deposit precursors for both kinetic and equilibrium models with various inlet velocities at 900 °C and $\gamma = 1$.

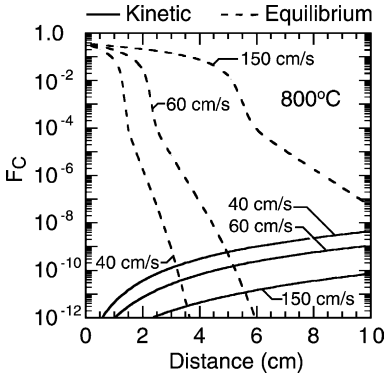

Fig. 10. Profiles of fractional carbon content in deposit precursors for both kinetic and equilibrium models with various inlet velocities at 800 °C and $\gamma = 0$.

4. Summary

We have developed a modified plug-flow model to analyze both the homogeneous kinetic and equilibrium chemistry in an anode flow channel of a DECO-SOFC. This model accounts for the effects of electrochemical oxidation of hydrocarbon fuel on both transport processes and reaction kinetics. While the reaction processes in these systems also involve complex heterogeneous chemistry, focusing on the gas-phase kinetics and equilibrium provides an essential first step toward understanding fuel chemistry. While the results presented here are for dry natural gas, the model can be readily extended to other hydrocarbon fuels such as propane and butane.

The homogeneous kinetics and equilibrium models show an interesting crossover in coking propensity. Near the channel entrance, where there is relatively little oxygen content, the equilibrium prediction shows high coking propensity. However, owing to relatively slow reaction rates, the kinetic predictions show small concentrations of coking precursors early in the channel. In downstream regions of the channel, the situation changes. With increasing levels of oxygen (primarily in the form of H_2O and CO_2), chemical equilibrium favors volatile carbon compounds and deposit formation. However, again owing to the relatively slow homogeneous reaction chemistry, the kinetics prediction continues to show increasing levels of coking precursors. The crossover point depends on operating temperature, fuel flow rate (residence time), and the rates of electrochemical reaction. The crossover behavior suggests that there may be ways to use spatially distributed catalysts that selectively promote equilibrium later in the channels where equilibrium suppresses coking. Practical implementation of this approach, however, would likely be difficult. The functional dependence of current density on fuel concentration strongly influences the tendency to foul porous anode structures. Higher values of γ will increase both kinetic and equilibrium coking propensity, with a much greater increase in the kinetic prediction. The higher order dependence also decreases

the average power density of the cell, as current density decreases with fuel depletion. Temperature also has a significant influence on molecular weight growth chemistry, increasing both precursor production rates and the equilibrium concentration of cyclic species and multi-ring aromatic hydrocarbons.

Acknowledgements

This work was supported by the DoD Multidisciplinary University Research Initiative (MURI) program administered by the Office of Naval Research under Grant N00014-02-1-0665 and also by the DARPA Palm Power initiative in collaboration with ITN Energy Systems. We gratefully acknowledge Neal Sullivan and Bill Barker at ITN Energy Systems for their help in this effort.

References

[1] R.J. Gorte, S. Park, J.M. Vohs, C. Wang, Anodes for direct oxidation of dry hydrocarbons in a solid-oxide fuel cell, Adv. Mater. 12 (2000) 1465–1469.
[2] K. Akihama, Y. Takatori, K. Inagaki, S. Sasaski, A.M. Dean, Mechanism of the smokeless rich diesel combustion by reducing temperature, in: Proceedings of the 2001 SAE World Congress, Detroit, 2001, No. 2001-01-0655, Society of Automotive Engineers.
[3] J. Koh, B. Kang, H.C. Lim, Y. Yoo, Thermodynamic analysis of carbon deposition and electrochemical oxidation of methane for SOFC anodes, Electrochem. Solid-State Lett. 4 (2001) A12–A15.
[4] E. Perry Murray, T. Tsai, S.A. Barnett, A direct-methane fuel cell with a ceria-based anode, Nature 400 (1999) 651–659.
[5] R.J. Kee, P. Korada, K. Walters, M. Pavol, A generalized model of the flow distribution in channel networks of planar fuel cells, J. Power Sources 109 (2002) 148–159.
[6] H. Zhu, R.J. Kee, A general mathematical model for analyzing the performance of fuel-cell membrane–electrode assemblies, J. Power Sources 117 (2003) 61–74 .
[7] M. Iwata, T. Hikosaka, M. Morita, T. Iwanari, K. Ito, K. Onda, Y. Esaki, Y. Sasaki, S. Nagata, Performance analysis of planar-type unit SOFC considering current and temperature distributions, Solid State Ionics 132 (2000) 297–308.
[8] R.S. Larson, PLUG: a program for the analysis of plug-flow reactors with gas-phase and surface chemistry, Technical Report SAND 96-8211, Sandia National Laboratories, 1996
[9] M.E. Coltrin, R.J. Kee, F.M. Rupley, E. Meeks, Surface Chemkin-III: a Fortran package for analyzing heterogeneous chemical kinetics at a solid-surface–gas phase interface, Technical Report SAND 96-8217, Sandia National Laboratories, 1996.
[10] R.J. Kee, F.M. Rupley, E. Meeks, J.M. Miller, Chemkin-III: A fortran chemical kinetics package for the analysis of gas-phase chemical and plasma kinetics, Technical Report SAND 96-8216, Sandia National Laboratories, 1996.
[11] C.A. Mims, R. Mauti, A.M. Dean, K.D. Rose, Radical chemistry in methane oxidative coupling: tracing of ethylene secondary reactions with computer models and isotopes, J. Phys. Chem. 98 (50) (1994) 13357–13372.
[12] A.Y. Chang, J.W. Bozzelli, A.M. Dean, Kinetic analysis of complex chemical activation and unimolecular dissociation reactions using QRRK theory and the modified strong collision approximation, Zeit. Phys. Ch. 214 (2000) 1533–1568.
[13] A.M. Dean, J.W. Bozzelli, Combustion chemistry of nitrogen, in: W.C. Gardiner Jr. (Ed.), Gas-Phase Combustion Chemistry, Springer, Berlin, 2000, pp. 125–341.
[14] D.L. Baulch, C.J. Cobos, R.A. Cox, C. Esser, P. Frank, T. Just, J.A. Kerr, M.J. Pilling, J. Troe, R.W. Walker, J. Warnatz, Evaluated kinetic data for combustion modeling, J. Phys. Chem. Ref. Data 21 (3) (1992) 411–734.
[15] M. Frenklach, J. Warnatz, Detailed modeling of PAH profiles in a sooting low-pressure acetylene flame, Combust. Sci. Technol. 51 (1987) 265–283.
[16] E.R. Ritter, J.W. Bozzelli, THERM: thermodynamic property estimation for gas phase radicals and molecules, Int. J. Chem. Kinet. 23 (1991) 767–778.
[17] T.H. Lay, J.W. Bozzelli, A.M. Dean, E.R. Ritter, Hydrogen atom bond increments for calculation of thermodynamic properties of hydrocarbon radical species, J. Phys. Chem. 99 (39) (1995) 14514–14527.
[18] K.E. Brenan, S.L. Campbell, L.R. Petzold, Numerical Solution of Initial-Value Problems in Differential Algebraic Equations, second ed., SIAM, Philadelphia, PA, 1996.
[19] U.M. Ascher, L.R. Petzold, Computer Methods for Ordinary Differential Equations and Differential-Algebraic Equations, SIAM, Philadelphia, PA, 1998.
[20] A.E. Lutz, F.M. Rupley, R.J. Kee, W.C. Reynolds, EQUIL: a program for computing chemical equilibria, Technical report, Sandia National Laboratories, 1996.
[21] W.C. Reynolds, The element potential method for chemical equilibrium analysis: implementation in the interactive program STANJAN-III, Technical report, Department of Mechanical Engineering, Stanford University, 1986.